Computers in Biology and Medicine 104 (2019) 97–104

Contents lists available at ScienceDirect

Computers in Biology and Medicine

journal homepage: www.elsevier.com/locate/compbiomed

A neural network approach to analyze cross-sections of muscle fibers in pathological images

Ye Li[a], Zhong Yang[b], Yaming Wang[c], Xinhua Cao[d], Xiaoyin Xu[e,*]

[a] Department of Electrical and Computer Engineering, Whiting School of Engineering, Johns Hopkins University, Baltimore, MD, USA
[b] Department of Clinical Hematology, Southwestern Hospital, Third Military Medical University (Army Medical University), Chongqing, China
[c] Department of Anesthesia, Brigham and Women's Hospital, Boston, MA, USA
[d] Department of Radiology, Boston Children's Hospital, Boston, MA, USA
[e] Department of Radiology, Brigham and Women's Hospital, Boston, MA, USA

ARTICLE INFO

Keywords:
Computer-aided analysis
Segmentation
Neural network
Muscle fibers
Cross-sections
Microscopic images

ABSTRACT

Morphological characteristics of muscle fibers, such as their cross-sections, are important indicators of the health and function of the musculoskeletal system. However, manual analysis of muscle fiber morphology is a labor-intensive and time-consuming process that is prone to errors. Overall, the procedure involves high inter- and intra-observer variability. Therefore, it is desirable for biologists to have a tool that can produce objective and reproducible analysis for muscle fiber images. In this work, we propose a deep convolutional neural network (DCNN) followed by post-processing for detecting and measuring the cross-sections of muscle fibers. We evaluate three segmentation networks for muscle boundary segmentation: (1) U-net, (2) FusionNet, and (3) a customized FusionNet. The customized FusionNet, which had the highest Dice coefficient on the test set, was used for subsequent morphological analysis of the muscle fibers. The proposed method was tested on microscopic images of the tibialis anterior muscles of a pre-clinical model of muscular dystrophy. The dataset contained four mosaic images, totalling more than 3400 fibers. Because of the severity of muscle injury in this pre-clinical model, its muscle fiber images present a challenge for quantitative analysis for several reasons. First, the muscle fibers had inhomogeneous spatial distribution and very different sizes. Second, the membranes of the muscle fibers had uneven signal intensity due to the loss of a membrane protein. Third, the shapes of intact muscle fibers were very different. All these factors contributed to the difficulty of acquiring good training data in the first place. Despite these difficulties, we achieved an average muscle fiber overlay precision of 0.65 and an average recall of 0.49. In this context, overlaid fibers are defined as fibers that have one or more pixels overlaying in the manual and DCNN cross-section segmentation. For the overlaid fibers, the proposed method achieved excellent segmentation accuracy of 94% ± 10.26%, as measured by the Dice-Sorensen coefficient.

1. Introduction

There are more than 40 diseases related to the dysfunctions of skeletal muscles, ranging from Duchenne muscular dystrophy (DMD) to muscle myopathies [1,2], with the key characteristic of muscular dystrophy being the lack of a membrane protein called dystrophin. This deficiency causes the muscle fiber to have a porous membrane and eventually to lose its cytoplasm. Morphologies of the cross-sections of muscle fibers provide important information about the health of a muscle and, more importantly, its capacity to regenerate new muscle fibers in the case of disease- or injury-caused damage [3]. However, due to the large number of objects, manual analysis of muscle fiber images is not only laborious but also subject to inter- and intra-observer variability.

Computer-aided analysis is a promising solution in muscle fiber detection and segmentation for its objective and quantitative measurements. Researchers have proposed various techniques to segment the muscle fiber boundary for muscle fiber segmentation. Most of these methods follow a multi-step image processing approach and adopt a combination of the following steps: (1) image enhancement to correct defects and uneven staining quality, (2) seed detection to find the centers of the muscle fibers, and (3) boundary segmentation. Representative boundary segmentation methods used in muscle fiber image processing include Otsu's method [4], k-means segmentation, deformable models [5], watershed segmentation [6], active contours, and graph cut and the variations and improvements of each method. In

* Corresponding author.
E-mail address: xxu@bwh.harvard.edu (X. Xu).

https://doi.org/10.1016/j.compbiomed.2018.11.007
Received 10 July 2018; Received in revised form 8 November 2018; Accepted 10 November 2018

addition, other methods have been developed by researchers to detect and segment cross-sections of muscle fiber. An early work by Briguet et al. in 2004 designed Feret's diameter as a means to measure the sizes of hundreds to thousands of muscle fibers seen in microscopic images [7]. However, the application of Feret's diameter depends on the segmentation of the muscle fibers. Hence, much effort has been dedicated to the segmentation and detection of the boundaries of muscle fibers. For example, Mula et al. proposed a method to first enhance the boundaries of muscle fibers by ridge detection and then use a gradient vector flow deformable model to delineate the boundaries of the seeded muscle fibers [8]. Sertel et al. applied a ridge detection method to segment the connective tissue components, which manifested as a bright curvilinear structure to segment muscle fibers [9]. Liu et al. proposed the adoption of a learning-based seed detection scheme to find the centers of the muscle fibers and then applied a deformable model to find the boundaries of the muscle fibers [10]. Janssens et al. designed a top-down multi-class support vector machine (SVM) scheme to segment muscle fibers in the steps of thresholding an image and classifying the segmentation into categories of individual muscle cells, clumps of muscle cells, and remnant connective tissues and then splitting the clumps of muscle cells into individual cells according to [11]. Smith and Barton proposed the use of a smooth filter to first suppress local minimums, followed by watershed transform to segment the boundaries of muscle fibers [6]. Wang et al. presented an approach to utilizing threshold selection, morphological ultimate erosion, and morphological dilation to find muscle fiber boundaries [12]. Combinations of image processing pipelines have also been proposed to segment muscle fiber boundaries. Voronoi and reversible jump Markov chain Monte Carlo has also been used for muscle fiber segmentation [13]. Miazaki et al. proposed an image-processing pipeline that consists of enhancement, noise reduction and binarization, and shape analysis of contours generated in the binarization process to detect muscle fiber boundaries [14]. Sapkota et al. developed a series of image-processing steps to find muscle fiber boundaries via automatic cell segmentation, perimysium annotation, and nuclei detection, followed by feature extraction and quantification to characterize the fibers [15]. Furthermore, Strange et al. presented a four-step approach to segment muscle fiber boundaries, namely, pre-processing to extract only the eosinophilic structures, coherence-enhancing diffusion filtering to enhance the boundaries, morphological operations to connect boundary regions, and watershed to split touching muscle fibers [16]. Deformable models have also been applied to find muscle fiber boundaries [5] but their performance depends on signal-to-noise ratio (SNR) of the images as a low SNR may cause the deformable models to break through the valid boundaries. The performance of deformable models can be improved if the process can be guided, as shown by Kim et al. [17] in which a level set approach was used to provide additional cues to the deformation process.

Although these existing techniques can obtain good results, their performances tend to deteriorate when the underlying images have low SNR, high heterogeneity in fiber size, and close adjacency between muscle fibers – a situation that we often encounter in practice. In fact, in musculoskeletal disease research, it is common to witness muscle specimens that contain broken fiber boundaries or extremely unevenly distributed muscle fibers, or both. From a biomedical research perspective, such scenarios may offer important insights into the mechanisms of musculoskeletal diseases, but we postulate that the existing methods may not be able to produce satisfying segmentation results in the challenging cases.

In this paper, we propose a deep convolutional neural network (DCNN) followed by post-processing for measuring cross-sections of muscle fibers in histopathological images with low SNR, uneven background, and close adjacency between muscle fibers. The cross-sections that we target for segmentation are the ones with muscle fiber boundaries that are 1) fully enclosed and 2) bright, which together is an indicator of the presence of dystrophin. These two conditions are required in our applications to differentiate the healthy muscle fibers, which tend to have consistently bright boundaries and fully enclosed boundaries, from the diseased ones, which tend to have broken boundaries or weakly stained boundaries due to the lack of even distribution of dystrophin. Thus, to segment such cross-sections, we must first find the muscle fiber boundaries that satisfy the aforementioned requirements.

2. Materials and methods

2.1. Animal experiments and image acquisition

We used a mouse model of muscular dystrophy to assess the health of the muscle fibers. The work had been approved by our institutional animal care and use committee. Male mdx mice at the age of four to eight weeks were used to mimick muscular dystrophy, a genetic disease with no available treatment. All the animal experiments were conducted under the approval of our institutional animal care and use committee. We transplanted wild type myoblasts from C57BL6 mice to the hind legs of the mdx mice to evaluate how the transplanted myoblasts might survive in the host. Before the transplantation, the hind legs of the mdx mice were irradiated at 18 Gy for three consecutive days to mimick the damage seen in muscular dystrophy cases. Then 10^5 myoblasts were injected into the tibialis anterior (TA) muscle at three evenly distanced positions. The mdx mice were then maintained on regular rodent food and cycles of 12-h light and 12-h dark in our animal housing facility for observation. At different time points post cell transplantation (PCT), the mice were euthanized to enable harvesting of the TA muscles to investigate how they might regenerate muscle fibers. The harvested tissues were post-fixed, dehydrated, and then frozen in an optimal embedding temperature compound. The specimen was sectioned along the longitudinal axis of the muscle every 12 μm, starting from the mid-portion of the TA muscle, and mounted on slides. The slides were washed with phosphate buffered saline and blocked with 5% goad serum, incubated with a rabbit anti-dystrophin antibody, and then incubated with a goat anti-rabbit Cy3-conjugated secondary antibody. We imaged the slides using an Olympus inverted IX-70 microscope to scan the whole cross-section of a TA muscle. An individual image usually has a dimension of 800 × 600 with a pixel size of 0.7 μm. Approximately 20–30 images were collected with slight overlaps in all four directions to cover the whole cross-section of the TA muscle.

An image dataset was collected over four mdx mice from two groups, with two in each group. The first group of mice was euthanized at one month PCT while the second group was euthanized at three months PCT. From each mouse, we acquired images over the TA muscles from both hinder legs. Overall, the dataset consisted of four mosaics of images, with each mosaic corresponding to the histology of one TA muscle. Our biologists manually labeled the muscle fiber boundaries in the dataset.

2.2. Dataset and data augmentation

The four mosaic images and their manually segmented labels were divided into 200 × 200 patches, resulting in a total of 5136 patches in the dataset. We used windowing to map the images' pixel value to a range from 0 to 255 and then up-sampled the images to 256 × 256. Each mosaic image consisted of 13–28 individual images, depending on the size of the specimen. In our data, the sizes of mosaic images were in the range of 1400 × 1900 pixels to 4800 × 5900 pixels. Fig. 1 shows several zoomed-in regions of an original muscle fiber image with manually marked intact cross-sections.

We implemented the augmentation method as described in Ref. [18] and augmented the training data with eight variations of image orientations. Fig. 2 shows an example of a training image and its augmented counterparts.

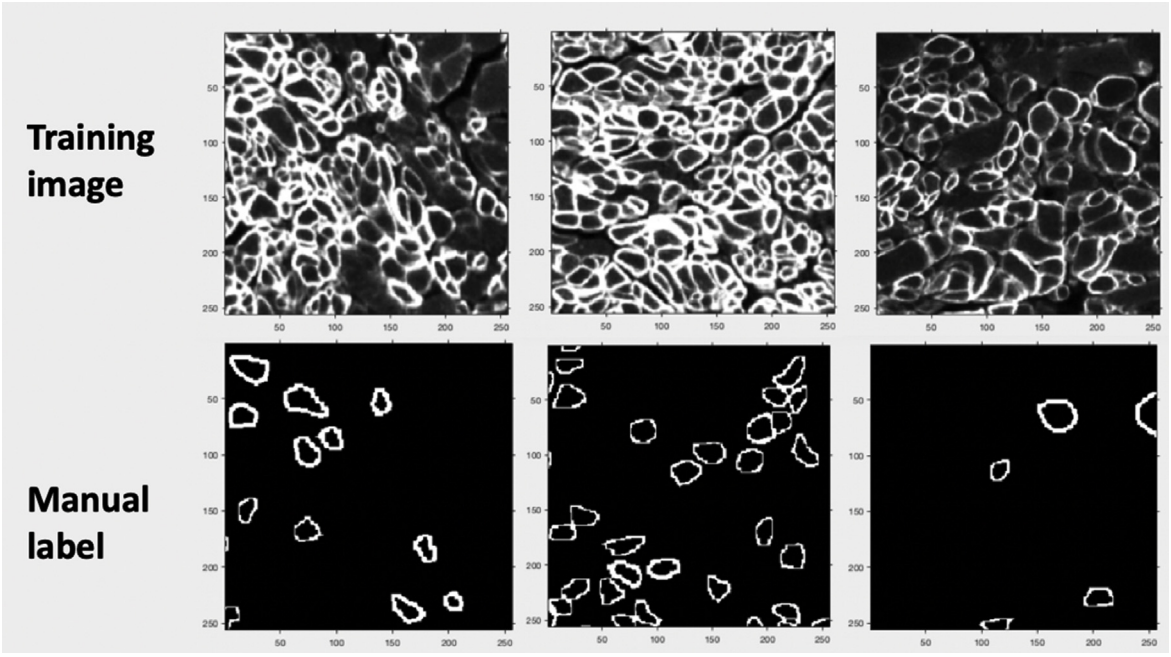

Fig. 1. Sample training images randomly drawn from the training data set. The top row comprises the input images to the DCNN and the bottom row shows the corresponding manual label (segmentation of the muscle fiber boundaries). The dimension of the input image is 256 × 256. Scale bar = 100 μm.

2.3. Network architecture selection

We evaluated three segmentation networks for muscle boundary segmentation: (1) U-net [19], (2) FusionNet [18], and (3) a customized FusionNet. We randomly selected 4300 patches from the 5136 patches and split the data with a 0.8–0.2 train-to-validation ratio for evaluating the performance of these networks. The training set was augmented as

Table 1
Dice coefficients of different network architectures.

Method	Dice coefficient
U-Net	0.3474
FusionNet	0.3516
Customized FusionNet	0.3704

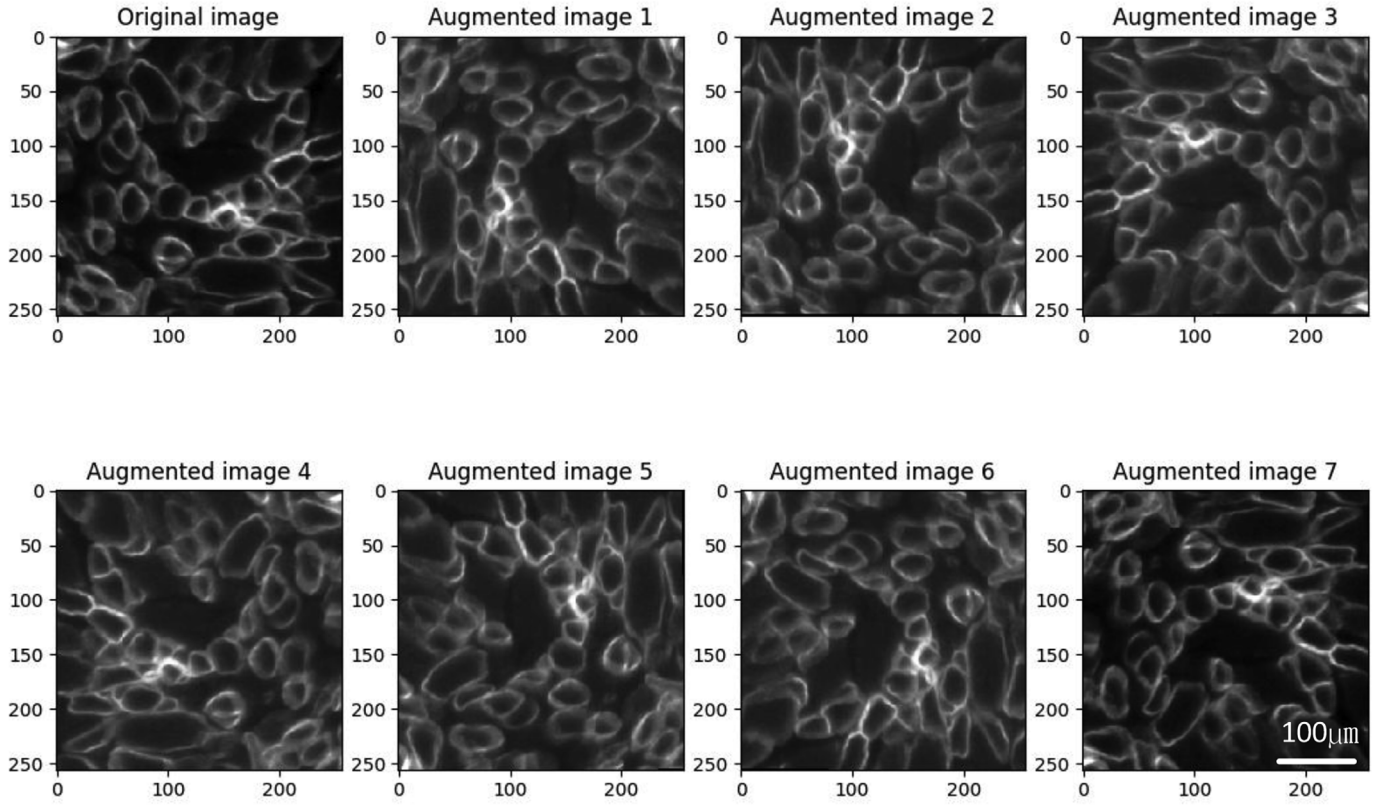

Fig. 2. A sample of the input image and its augmented counterparts. By collecting this, we increase the training data size by eight times.

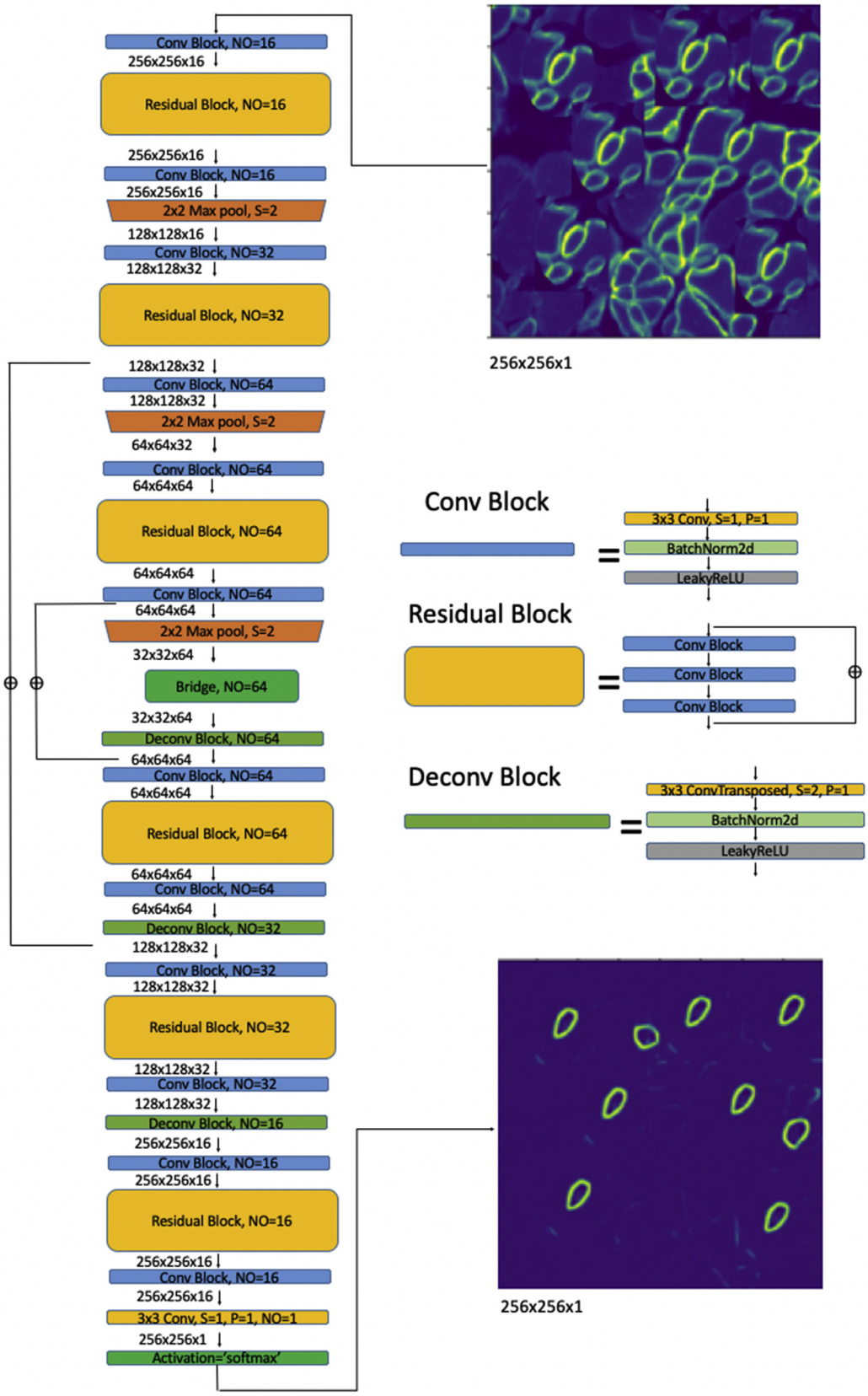

Fig. 3. Proposed network architecture optimized for segmentation of muscle fiber boundaries.

described in Section 2.2. The Dice coefficient was used to gauge the performance of the network. The comparison result from one mosaic image is shown in Table 1. The network architecture that produced the highest Dice coefficient, in this case, the customized FusionNet, was selected for subsequent morphological analysis of the muscle fibers.

2.4. Architecture of proposed segmentation network

The proposed network architecture is built upon the FusionNet [18]. We combine the modified architecture with the exponential logarithmic loss function in Ref. [20] to improve the segmentation of small objects.

The dimensions of the feature maps from each layer are shown in Fig. 3. The encoder consists of 3 residual blocks, each sandwiched by 2 convolutional blocks and followed by a max-pooling layer. A convolutional block is composed of a 3×3 convolution layer with stride 1 and padding 1, a batch normalization layer, and an activation layer. Correspondingly, the decoder consists of 3 deconvolutional blocks, each followed by a convolutional block, a residual block, and another convolutional block. A deconvolutional block consists of a 3×3 transposed convolution layer with stride 2, padding 1, and output padding 1, a batch normalization layer, and an activation layer. Specifically, we have four modifications to the FusionNet: (1) we reduced the starting number of filters of the FusionNet from 64 to 16, (2) we implemented a *softmax* activation instead of the *tanh* activation at the end of the network, for use of the loss function proposed in Ref. [20], (3) we decreased the depth of the network; and (4) we reduced the number of summation-based skip connections. Combining these modifications reduced the network trainable parameters from almost 5 million to only 0.7 million and increased the Dice coefficient from 0.35 to 0.37.

We adopted the combined exponential logarithmic loss function in Ref. [20] to improve segmentation on small structures:

$$\mathscr{L} = \omega_{cross}\mathscr{L}_{cross} + \omega_{Dice}\mathscr{L}_{Dice} \tag{1}$$

where ω_{cross} and ω_{Dice} are the weights of the exponential categorical cross-entropy loss and the exponential logarithmic Dice loss, respectively, whereas

$$\mathscr{L}_{cross} = \mathrm{E}\left[(-\ln(p(x)))^{\beta_{cross}}\right] \tag{2}$$

where x represents the pixel position and $p(x)$ is the *softmax* probability, the network's predicted value for pixel at position x. Here E is the mean value with respect to x. The logarithmic Dice loss is defined as

$$\mathscr{L}_{Dice} = \mathrm{E}\left[(-\ln(\mathrm{Dice}))^{\beta_{\mathrm{Dice}}}\right] \tag{3}$$

and

$$\mathrm{Dice} = \frac{2(\sum_x y(x)\mathrm{p}(\mathrm{x})) + \varepsilon}{(\sum_x y(x) + p(\mathrm{x})) + \varepsilon} \tag{4}$$

where $y(x)$ is the ground truth segmentation of the muscle fiber boundaries, which is 1 when the pixel x is on a boundary and 0 otherwise. In Eq. (4), $\varepsilon = 1$ is a smoothing constant to handle images with no ground truth labels in the training samples. β_{Dice} and β_{Cross} are hyper-parameters that control the nonlinearities of the loss functions. We set $\beta_{\mathrm{Dice}} = \beta_{\mathrm{Cross}} = 0.3$ as suggested by Ref. [20].

2.5. Post-processing of DCNN output

We processed the output from the proposed DCNN in three steps. First, we used a flat, disk-shaped structuring element to close any small gaps that may exist in the DCNN output. The radius that we used for the disk is 2 pixels. Second, we filled any holes in the output image from step one. Third, we subtracted the output image of step one from the resulting image of step two. Fig. 4 shows the post-processing results on a challenging testing image patch that had both clustered objects and inhomogeneous signal intensity.

2.6. Robustness of the proposed network

To evaluate the robustness of our proposed network, we designed four experiments to test the network's ability to recognize 1) an already learned pattern at a different location in the image, 2) a slightly and a significantly rotated version of an already learned pattern, 3) an already learned pattern with decreased contrast, and 4) an unenclosed version of an already learned enclosed pattern. As shown in the testing results, the proposed network can recognize the learned pattern at several different locations in the image as well as a slight rotated version of the learned pattern. In addition, the network can also omit recognition of the unenclosed and the lower contrast version of the already learned pattern. The segmented results were both weak and unenclosed in these cases, indicating that partial activation of the learned pattern was present in some of the feature maps. Here, a complete activation refers to a full light-up of all the neurons that were needed to reconstruct the learned pattern. We evaluated the proposed neural network through both qualitative and quantitative comparisons with manual segmentation. We applied the proposed neural network to analyze and compare the mosaic images from each group. It can be observed that the proposed method learns to segment the entire structure of the muscle fiber boundaries. Fig. 5 shows examples of the simulated testing images and their testing results.

2.7. Training strategy

The image augmentation method introduced in Section 2.2 was used to learn invariant features to avoid overfitting. All the weights in the model were made trainable. The optimizer Adam was used with a learning rate of 10^{-3}, batch size of 35, and 100 epochs. The proposed model was implemented in Keras on an NVIDIA TITAN X GPU with 12 GB memory.

3. Results

3.1. Morphological analysis of muscle fibers

The proposed network was used to perform the morphological analysis of the muscle fibers using a leave-one-out method through selection of three mosaic images as the training set and the remaining one as a testing set. This process was repeated with each mosaic image in turn, resulting in four testing results. To evaluate the proposed network's performance quantitatively, we adopted a set of metrics, including the total number of muscle fibers, the mean and standard deviation of the area of muscle fibers, and mosaic overlay precision and recall. In this context, overlaid fiber is defined as having one or more pixels overlaying in its manual and DCNN cross-section segmentation. The mosaic overlay precision is equal to the number of overlaid fibers in a mosaic image (true positives) divided by the total number of fibers segmented by the DCNN (true positives + false positives). The mosaic overlay recall is equal to the number of overlaid fibers in a mosaic image (true positives) divided by the sum of the number of overlaid fibers and the number of the fibers that are segmented by the manual label but are not segmented by the DCNN (true positives + false negatives).

3.2. Quantitative results

The quantitative results of the morphological analysis are shown in Table 2. In our context, an optimal model is one that provides the most distinguishing power between the three-month PCT group and the one-month PCT group. To measure the distinction, we computed the absolute mean group-difference between the manually labeled results and those given by our proposed method. In this context, the absolute mean group-difference is defined as the difference between the mean number of fibers in the three-month PCT and that of the one-month PCT. As

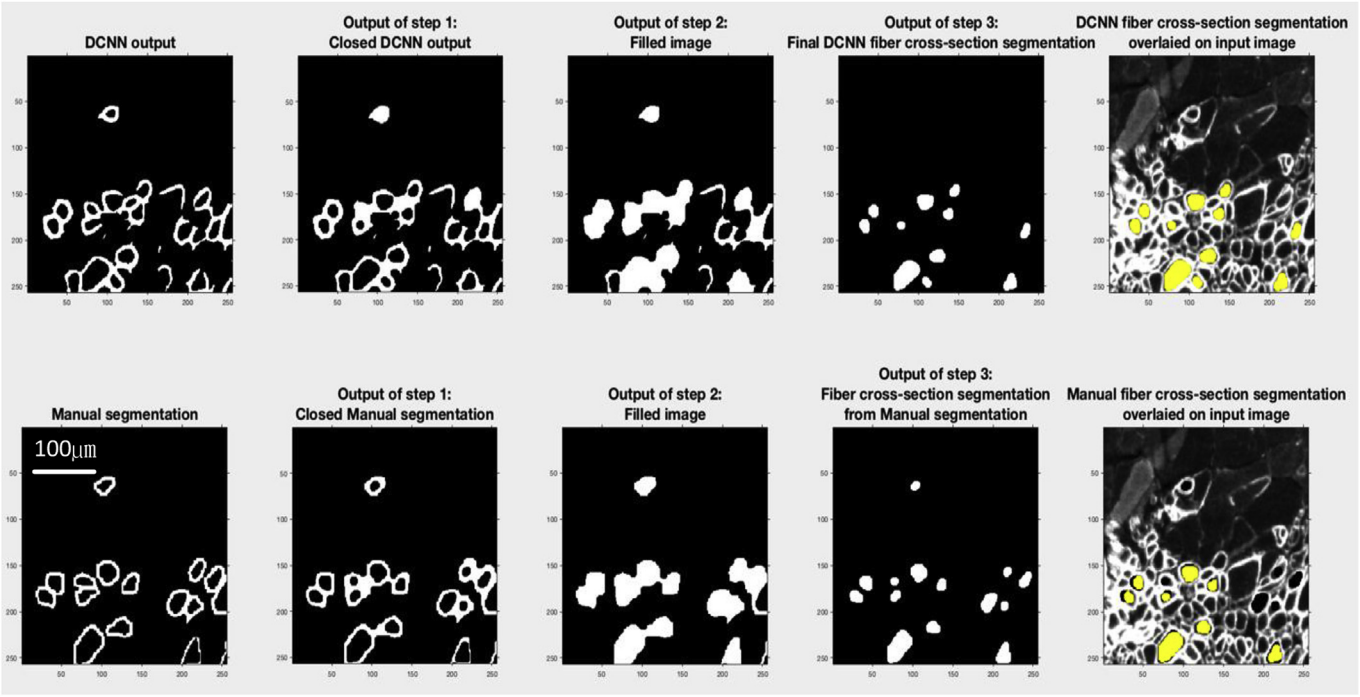

Fig. 4. Segmentation results of a challenging image patch selected from our testing dataset. From left to right, the top row presents the segmented muscle fiber boundaries by DCNN; output image from post-processing steps 1, 2, 3; and the segmented cross-sections overlaid on top of the input image. The bottom row shows their corresponding counterparts by manual analysis.

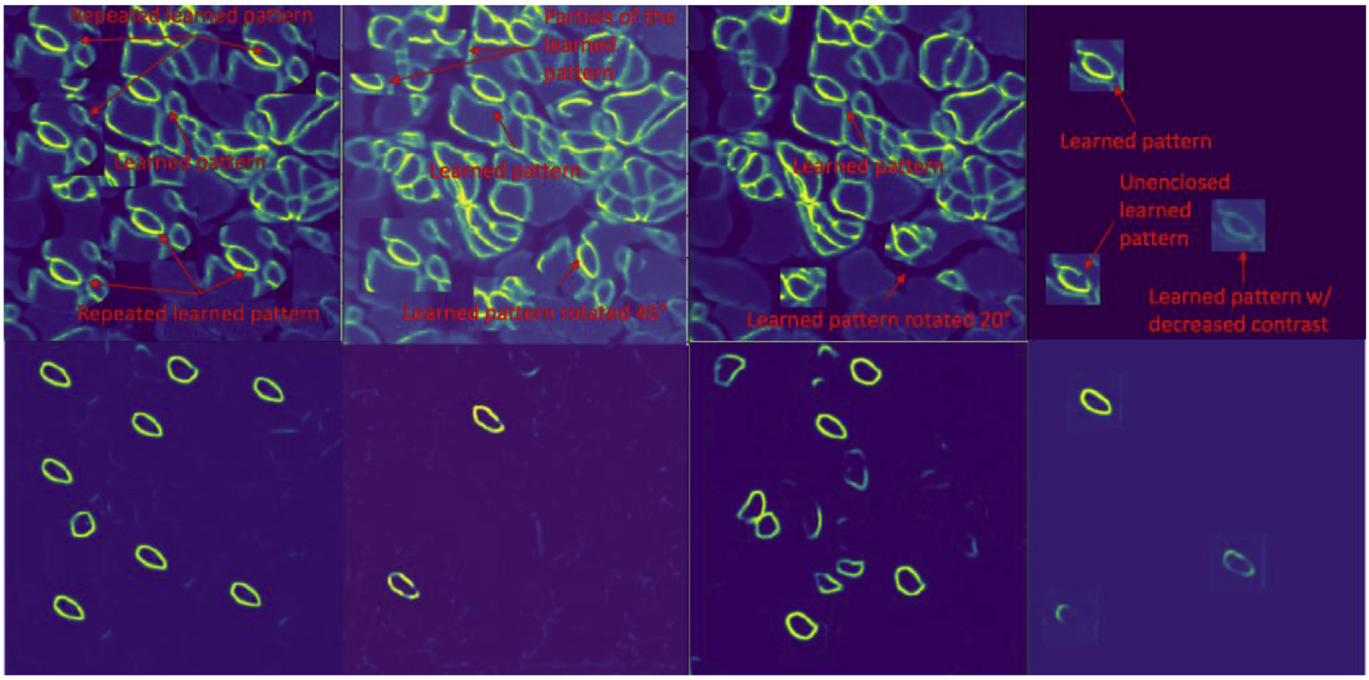

Fig. 5. Examples of simulated testing images for testing the proposed network architecture. From left to right, the top row shows the simulated images for testing the network's ability to: 1) recognize an already learned pattern at a different location in the image, 2) recognize a significantly rotated version of an already learned pattern, 3) recognize a slightly rotated version of an already learned pattern, and 4) recognize an unenclosed version of an already learned enclosed pattern and an already learned pattern with decreased contrast. The bottom row is the testing results with the proposed network structure.

expected, as a result of the treatment intervention, the three-month PCT group had more healthy muscle fibers. Also, areas of muscle fibers of the three-month PCT group were larger than those of the one-month PCT group, indicating that the transplanted cells regenerated healthy muscle fibers to grow over time. For the detected fibers, the proposed method achieved excellent segmentation accuracy of 94% ± 10.26%, as measured by the Dice-Sorensen coefficient. When comparing the results given by the neural network with those from manual analysis, the absolute mean group-difference is 1427 for the proposed method and 544 for the manually segmented results. It can be observed that the proposed neural network can distinguish mosaic images between the two groups. In terms of comparing the results given by the neural

Table 2
Morphological analysis results of mosaic images at three-month and one-month PCT.

	Three month PCT		One month PCT	
	Specimen 1	Specimen 2	Specimen 3	Specimen 4
DCNN detected number of fibers	2173	1335	389	266
Manually labeled number of fibers	1243	1006	483	678
DCNN detected muscle fiber area (mean)	170.43	145.78	158.58	172
Manually labeled muscle fiber area (mean)	279.56	245.31	220.7	529
DCNN detected muscle fiber area (STD)	158.18	138.32	177.1	113
Manually labeled muscle fiber area (STD)	222.73	279.75	305.34	455
Mean Dice for overlaid fibers	0.9512 ± 0.1015	0.9428 ± 0.0973	0.9295 ± 0.1136	0.9358 ± 0.0978
Mosaic overlay precision	0.4054	0.6	0.72	0.891
Mosaic overlay recall	0.4154	0.63	0.55	0.3553

network and manual analysis, we note that the discrepancies may arise from two perspectives. First, there was high inter- and intra-observer variation in the manual analysis in selecting valid muscle fibers, and this variation affects the consistency in ground-truth as provided by a human observer. Second, in tracing the boundary of a muscle fiber to furnish the training dataset, there was also variation in manually marking the boundary. While a human observer can be very robust in determining which objects are valid muscle fibers, the use of a pointing device to trace the muscle fiber boundaries is often an inconsistent and time-consuming procedure. This variation also affects the quality of the training dataset for the purposes of tuning the neural network. Despite the above compounding factors, we note that, from each example given in Table 1, the areas of muscle fibers given by the neural network had a smaller standard deviation than those given by manual analysis, pointing to the advantage of a neural network in generating a more consistent measurement in analyzing complex shapes.

4. Discussion

Because of the large number of muscle fibers observed in a field of view in microscope imaging, their labeling done manually is time-consuming and subject to observers' bias. Over the last twenty to thirty years, computerized analysis—conducted to replace or augment manual methods—of muscle fiber images has been under active development. These methods, ranging from global thresholding [4] and watershed [6] to level set [21], and deformable models [5,10], have achieved various degree of success. However, one limitation of the existing methods is that they tend to work well on images of high SNR and intact muscle fiber boundaries. Though this limitation does not hinder the usage of existing methods on healthy and normal muscle fiber specimens, these methods may achieve sub-optimal performance on diseased models of musculoskeletal conditions. From a research perspective, often one needs to work with diseases models to gain insight into the pathophysiology of muscular dystrophies and other disorders. For example, one prominent feature of several muscular dystrophy disorders is the loss of certain membrane protein. To study how the affected muscle fibers may retain or regain the membrane protein in response to therapies, we need to label the muscle fibers with the corresponding antibody and the acquired images then may have uneven signal intensity due to the fact that the healthy muscle fibers demonstrate strong and even expression of the antibody while the diseased muscle fibers have low and uneven expression. This phenomenon can render the existing methods unsuitable for analyzing and quantifying muscle fibers in some applications. We proposed a neural network approach that can be trained to recognize muscle fibers in challenging cases. As the neural network is trained on individually delineated muscle fibers, it can avoid some caveats in finding valid muscle fibers. For example, it can avoid the inter-fiber spaces and non-convex contours.

To the best of our knowledge, our work is the first to focus on severely diseased models of muscular dystrophies. The complexity of our data arises from the fact that, in a diseased model of musculoskeletal disorders, the muscle fibers are often damaged and do not have a uniform appearance, in contrast to healthy muscles. This complexity makes it very challenging to collect good training data.

5. Conclusions

As many musculoskeletal diseases are characterized by the destruction of muscle fiber membranes, it is imperative for researchers to have computer-aided analysis techniques to evaluate muscle fibers at the microscopic scale for objective and quantitative comparisons. However, challenges arise, as there is a large variation in the geometrical and morphological distribution of muscle fibers, particularly in diseased muscle fibers. In this work we introduced a neural network approach to analyze the histopathological images to identify muscle fibers that have contact expression of dystrophin on their membranes, an indicator of their health. From a computational perspective, the approach is applicable to similar images regardless of how the membranes are labeled. As a training-based technique, the proposed approach depends on the availability of the marked ground truth. In practical application, the approach's performance will largely depend on the quality and quantity of the training data. Here we note that, as shown in the results, the performance of the neural network depended largely on the quantity of the training data, and, in particular, the number of morphological shapes that were available in the training data. We also showed several variations of a learned pattern in our simulated experiments and, through those experiments, we observed that, if the testing pattern differed from any of the training patterns by a large degree, the proposed network would not recognize the new pattern. The underlying task of detecting and segmenting muscle fiber cross-sections is very challenging, because the muscle fibers manifest a large variation of morphologies and have close adjacency to each other. In addition, in our biology study, only the healthy muscle fibers have an enclosed boundary and consistent signal intensity along the boundary. Many diseased muscle fibers have very similar shapes and similar signal intensities, making them difficult to differentiate from healthy fibers. In this work, we developed the neural network approach for focusing on a single channel image of the membranes of muscle fibers. The distribution of nuclei provides additional information about the health of muscle fibers, and the nuclei can be imaged in a different channel [22]. It is beneficial to develop computer-aided analysis of both channels to gain insight into how muscle fibers may survive and regenerate in cell therapy, as mature fibers have nuclei distributed peripherally, and newly regenerated fibers have centrally located nuclei [23].

Author declaration

None Declared.

Acknowledgements

Y. Li was supported by the NIH award R01LM011415. Z. Yang was supported by the National Science Foundation of China award 31571242. X. Cao was supported by the NIH award R01LM012434. X. Xu was supported by the NIH awards R01LM011415 and R01LM012434.

References

[1] P. Gregorevic, J.S. Chamberlain, Gene therapy for muscular dystrophy - a review of promising progress, Expet Opin. Biol. Ther. 3 (5) (2003) 803–814.
[2] A.E. Emery, The muscular dystrophies, Lancet 359 (9307) (2002) 687–695.
[3] H.W. Venema, J. Overweg, Analysis of size and shape of cross-sections of muscle-fibers, Med. Biol. Eng. 12 (5) (1974) 681–692.
[4] M.P. de Melo, J.C. Felipe, An approach for segmentation of skeletal muscle fibers in histological images, XIII Congresso Brasileiro em Informática em Saúde, 2012.
[5] A. Klemenčič, S. Kovačič, F. Pernuš, Automated segmentation of muscle fiber images using active contour models, Cytometry: J. Int. Soc. Anal. Cytol. 32 (4) (1998) 317–326.
[6] L.R. Smith, E.R. Barton, SMASH–semi-automatic muscle analysis using segmentation of histology: a MATLAB application, Skeletal Muscle 4 (1) (2014) 21.
[7] A. Briguet, I. Courdier-Fruh, M. Foster, T. Meier, J.P. Magyar, Histological parameters for the quantitative assessment of muscular dystrophy in the mdx-mouse, Neuromuscul. Disord. 14 (10) (2004) 675–682.
[8] J. Mula, J.D. Lee, F.J. Liu, L. Yang, C.A. Peterson, Automated image analysis of skeletal muscle fiber cross-sectional area, J. Appl. Physiol. 114 (1) (2013) 148–155.
[9] O. Sertel, B. Dogdas, C.S. Chiu, M.N. Gurcan, Microscopic image analysis for quantitative characterization of muscle fiber type composition, Comput. Med. Imaging Graph. 35 (7–8) (2011) 616–628.
[10] F. Liu, A.L. Mackey, R. Srikuea, K.A. Esser, L. Yang, Automated image segmentation of haematoxylin and eosin stained skeletal muscle cross-sections, J. Microsc. 252 (3) (2013) 275–285.
[11] T. Janssens, L. Antanas, S. Derde, I. Vanhorebeek, G. Van den Berghe, F. Guiza Grandas, Charisma: an integrated approach to automatic H&E-stained skeletal muscle cell segmentation using supervised learning and novel robust clump splitting, Med. Image Anal. 17 (8) (2013) 1206–1219.
[12] Z. Wang, A semi-automatic method for robust and efficient identification of neighboring muscle cells, Pattern Recogn. 53 (2016) 300–312.
[13] I.L. Dryden, R. Farnoosh, C.C. Taylor, Image segmentation using Voronoi polygons and MCMC, with application to muscle fibre images, J. Appl. Stat. 33 (6) (2006) 609–622.
[14] M. Miazaki, M.P. Viana, Z. Yang, C.H. Comin, Y. Wang, F.C.L. da, X. Xu, Automated high-content morphological analysis of muscle fiber histology, Comput. Biol. Med. 63 (2015) 28–35.
[15] M. Sapkota, F.Y. Xing, H. Su, L. Yang, Automatic muscle perimysium annotation using deep convolutional neural network, 2015 IEEE 12th International Symposium on Biomedical Imaging (ISBI), 2015, pp. 205–208.
[16] H. Strange, I. Scott, R. Zwiggelaar, Myofibre segmentation in H&E stained adult skeletal muscle images using coherence-enhancing diffusion filtering, BMC Med. Imag. 14 (2014) 38.
[17] Y.J. Kim, T. Brox, W. Feiden, J. Weickert, Fully automated segmentation and morphometrical analysis of muscle fiber images, Cytometry A 71 (1) (2007) 8–15.
[18] T.M. Quan, D.G.C. Hildebrand, W.-K. Jeong, FusionNet: A deep fully residual convolutional neural network for image segmentation in connectomics, ArXiv e-prints 2016 cited 1612; Available from: http://adsabs.harvard.edu/abs/2016arXiv161205360Q.
[19] O. Ronneberger, P. Fischer, T. Brox, U-net: convolutional networks for biomedical image segmentation, Med. Imag. Comput. Computer-Assist. Intervention 9351 (Pt Iii) (2015) 234–241.
[20] K.C.L. Wong, M. Moradi, H. Tang, T. Syeda-Mahmood, 3D Segmentation with Exponential Logarithmic Loss for Highly Unbalanced Object Sizes, Springer International Publishing, 2018, pp. 612–619 Cham %@ 978-3-030-00931-1.
[21] A. Sáez, A. Montero-Sánchez, L.M. Escudero, B. Acha, C. Serrano, Segmentation of muscle fibres in fluorescence microscopy images, International Conference Image Analysis and Recognition, Springer, 2012, pp. 465–472.
[22] C.H. Comin, X. Xu, Y. Wang, F.L.d. Costa, Z. Yang, An image processing approach to analyze morphological features of microscopic images of muscle fibers, Comput. Med. Imaging Graph. 38 (8) (2014) 803–814.
[23] G. Ferrari, G. Cusella-De Angelis, M. Coletta, E. Paolucci, A. Stornaiuolo, G. Cossu, F. Mavilio, Muscle regeneration by bone marrow-derived myogenic progenitors, Science 279 (5356) (1998) 1528–1530.